Received: 29 July 2021 | Accepted: 27 June 2022

DOI: 10.1002/nme.7068

RESEARCH ARTICLE

WILEY

# Peridynamic bond-associated correspondence model: Reformulation and comparison study

**WaiLam Chan** | **Hailong Chen**

Mechanical Engineering Department, University of Kentucky, Lexington, Kentucky 40506, USA

**Correspondence**
Hailong Chen, Mechanical Engineering Department, University of Kentucky, Lexington, KY 40506, USA.
Email: hailong.chen@uky.edu

**Abstract**

The peridynamic bond-associated formulation has been shown to be effective in stabilizing the conventional correspondence model for both two-dimensional and three-dimensional, static, and dynamic problems. However, recent study revealed the persistence of material instability in the bond-associated formulation for one-dimensional problems for majority combinations of the bond associated horizon size and material point horizon size and two-dimensional problems when both the bond-associated horizon size and the material point horizon size are twice of mesh spacing. In addition, it was found that the bond-associated formulation has instability in dynamic problems when the bond-associated horizon size is close to the material point horizon size. In this article, a reformulation of the bond-associated correspondence formulation is presented. Distinct from the original formulation, the proposed reformulation derives the force density states of a bond as a volume weighted average of all bond-associated force density states whose bond-associated horizons include the material points of the bond. Similar to the original bond-associated formulation, the proposed reformulation recovers the conventional formulation when the bond-associated horizon size is at least twice as large as the material point horizon size. Detailed numerical study on wave dispersion relations, static deformation, and dynamic wave propagation problems are performed to investigate and compare the two bond-associated formulations. It is found that for all these three types of problems, the proposed reformulation significantly improves the model instability compared to the original bond-associated formulation, especially when the bond-associated horizon size is small relative to the material point horizon size. Based on numerical study, small bond-associated horizon is recommended for use in the proposed reformulation.

**KEYWORDS**

bond-associated formulation, instability, material correspondence models, peridynamics

## 1 | INTRODUCTION

The peridynamic correspondence formulation offers unique benefits in modeling nonlinear inelastic materials by directly incorporating material constitutive models from local continuum mechanics theory.[1] This is very appealing since it significantly facilitates modeling fracture of nonlinear inelastic materials within the peridynamics framework. However,

  

the conventional correspondence formulation suffers from some practical difficulties, such as material instability[2] and sub-horizon collapse and matter penetration.[3] Various stabilization techniques have been proposed to eliminate the material instability by introducing additional force density states, such as those based on non-uniform part of the deformation state,[2] bond-stretch informed strain tensor,[3] and corrected bond deformation.[4] A brief survey of different stabilization techniques can be found in Reference 5.

Among many stabilization techniques in the literature, the bond-associated formulations[5-12] use the concept of bond-associated horizon to inherently stabilize the conventional correspondence formulation without introducing additional material-dependent parameters. Different from the material point horizon (denoted as $H$), a bond-associated horizon (denoted as $h$) is a horizon defined at a material point but associated with a specific bond. For bond $\boldsymbol{\xi} = \mathbf{X}' - \mathbf{X}$ where $\mathbf{X}$ and $\mathbf{X}'$ are the Cartesian coordinates of two material points connected by the bond, the bond-associated horizon of bond $\boldsymbol{\xi}$ is defined at material point $\mathbf{X}'$ (denoted as $h_{\mathbf{X}'}$) and its size is usually different from the material point horizon at $\mathbf{X}'$ (denoted as $H_{\mathbf{X}'}$). Therefore, in addition to the material point horizon used in the conventional formulation, there is a bond-associated horizon corresponds to a bond in the bond-associated formulation. For the case of bond $\boldsymbol{\xi}$, these two horizons are material point horizon $H_{\mathbf{X}}$ and bond-associated horizon $h_{\mathbf{X}'}$. While the conventional formulation formulates the deformation gradient with the support of a material point horizon, for example, $H_{\mathbf{X}}$, for all bonds connect the material point, the bond-associated formulation constructs deformation gradient, also called as bond-associated deformation gradient, using a subset of a material point horizon that determined as the intersection of the material point horizon and the bond-associated horizon for each individual bond, for example, $H_{\mathbf{X}} \cap h_{\mathbf{X}'}$ for bond $\boldsymbol{\xi}$. When the bond-associated horizon is at least twice as large as the material point horizon, the subset becomes the whole material point horizon. Therefore, the deformation gradient constructed in the conventional formulation is recovered from the bond-associated deformation gradient under such condition. In addition to the change to the support of the deformation gradient construction, the bond-associated formulation also introduces a coefficient, which is determined as the volume ratio of the subset to the whole material point horizon, to localize the calculation of the force density state of a bond. As will be revealed in the numerical study of this work, this has the potential to cause numerical issue in the bond-associated formulation for small bond-associated horizon size relative to the size of material point horizon. In general, the force density state of a bond should depends on all the bond-associated force density states whose calculation involves the deformation state of the bond.

The bond-associated horizon concept was originally proposed by Chen and Spencer.[5,6] They showed the effectiveness of the bond-associated formulation in removing material instability and its good convergence characteristic using 2D and 3D static deformation problems. Later, Gu et al.[7] applied the bond-associated concept in combination with the peridynamic differential operator[13] to construct deformation gradient of higher-order accuracy in the correspondence formulation. Gu et al. numerically demonstrated the bond-associated formulation is effective in improving the prediction accuracy and removing the oscillations in the displacement field. Madenci et al.[8] formulated the weak form of the bond-associated formulation based on low-order deformation gradient (comparing to the higher-order approximation by Gu et al.[7]) constructed using peridynamic differential operator and showed that both essential and natural boundary conditions can be imposed employing the weak form. Roy et al.[10] applied the bond-associated formulation to study the elastic finite deformation and rupture in polymers. Behera et al.[9,11] applied the same bond-associated formulation to investigate the fracture of Neo-Hookean material under finite elastic deformation and viscoelastic material under finite deformation. Yang et al.[14] applied the bond-associated formulation incorporating the Johnson–Holmquist II constitutive damage model to study the severe damage of concrete under intense impact compression. Recently, Chan and Chen[12] conducted a detailed study of the bond-associated formulation proposed by Chen and Spencer[5] using wave dispersion analysis for all three dimensional problems. The study further confirmed the effectiveness of the bond-associated formulation for 2D and 3D problems. However, for 1D problems, there is still material instability for most of the combinations of the material point horizon size and the bond-associated horizon size. In an unpublished work by Chan and Chen, it was found that the bond-associated formulation has instability in dynamic problems when the bond-associated horizon size is close to the size of material point horizon. This instability will be demonstrated in the numerical study in this article.

In this article, we propose to reformulate the bond-associated formulation to significantly improve its stability for 1D problems and multi-dimensional problems when bond-associated horizon size is comparable to the material point horizon size. In the proposed reformulation, instead of using the volume ratio to localize its dependence, the force density state depends on all bond-associated force density states whose calculation involves the deformation state of a bond. This is achieved by distributing the energy of a material point horizon to all its subsets. The remainder of this article is organized as follows: Section 2 reviews the definition of bond-associated deformation gradient and the derivation of force density state in the original bond-associated formulation. Following this, the derivation of the proposed reformulation is

presented in Section 3. Similarity and difference between the proposed reformulation and the original formulation are discussed. In Section 4, parametric study to compare the two bond-associated formulations are conducted using three types of problems including wave dispersion analysis, static deformation analysis and wave propagation analysis. Discussions and conclusions are made in Section 5.

## 2 | REVIEW OF FORM I BOND-ASSOCIATED CORRESPONDENCE FORMULATION

For clarity, we call the bond-associated formulation originally proposed by Chen and Spencer[5,6] as Form I formulation, and the proposed bond-associated reformulation in this work as Form II formulation. This section briefly reviews the Form I formulation with focus on the bond-associated deformation gradient and force density state.

### 2.1 | Bond-associated deformation gradient

In Form I formulation,[5,6] the bond-associated deformation gradient is derived using the weighted least squares technique. However, the support for the bond-associated deformation gradient is a subset of the material point horizon instead of the whole material point horizon used in the conventional formulation (see Figure 1 for the intersection of material point horizon $H_{\mathbf{X}}$ and bond-associated horizon $h_{\mathbf{X}'}$ as $H_{\mathbf{X}} \cap h_{\mathbf{X}'}$). With a given subset of a material point horizon, the bond-associated deformation gradient for the corresponding bond $\boldsymbol{\xi} = \mathbf{X}' - \mathbf{X}$ can be calculated using

$$\mathbf{F}_{\xi} = \mathbf{k}_{\xi} \cdot \mathbf{K}_{\xi}^{-1}, \tag{1}$$

where

$$\mathbf{K}_{\xi} = \int_{H_{\mathbf{X}} \cap h_{\mathbf{X}'}} w\langle \boldsymbol{\xi}' \rangle \cdot \underline{\mathbf{X}}'\langle \boldsymbol{\xi}' \rangle \otimes \underline{\mathbf{X}}'\langle \boldsymbol{\xi}' \rangle dV_{\mathbf{X}''}, \tag{2}$$

is the bond-associated shape tensor in the reference configuration and

$$\mathbf{k}_{\xi} = \int_{H_{\mathbf{X}} \cap h_{\mathbf{X}'}} w\langle \boldsymbol{\xi}' \rangle \cdot \underline{\mathbf{Y}}'\langle \boldsymbol{\xi}' \rangle \otimes \underline{\mathbf{X}}'\langle \boldsymbol{\xi}' \rangle dV_{\mathbf{X}''}, \tag{3}$$

is the bond-associated shape tensor in the current configuration, with $w$ being the weight function, $\boldsymbol{\xi}' = \underline{\mathbf{X}}'\langle \boldsymbol{\xi}' \rangle = \mathbf{X}'' - \mathbf{X}$ being the relative position vector state between material points $\mathbf{X}''$ and $\mathbf{X}$ in the reference configuration $\Omega_r$, and $\underline{\mathbf{Y}}'\langle \boldsymbol{\xi}' \rangle =$

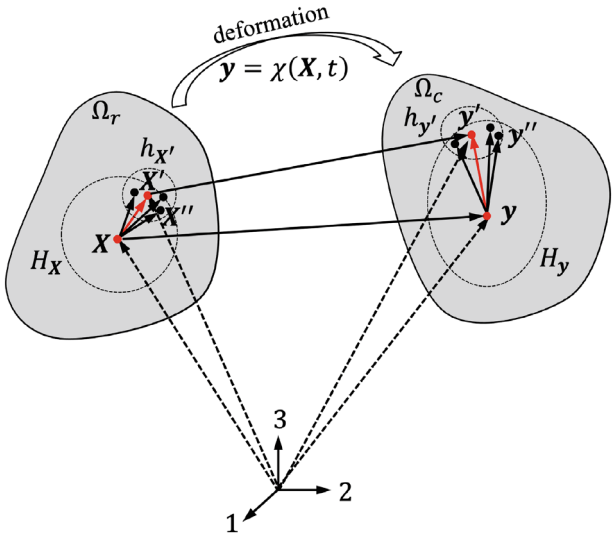


**FIGURE 1** Configuration for the construction of bond-associated deformation gradient

$\mathbf{y}'' - \mathbf{y}$ being the relative position vector state or deformation state between material points $\mathbf{X}''$ and $\mathbf{X}$ in the current configuration $\Omega_c$. $\mathbf{y}''$ and $\mathbf{y}$ are the current position of material points $\mathbf{X}''$ and $\mathbf{X}$, respectively. The angle bracket notation indicates the association of states.

Denoting the radius of material point horizon $H_{\mathbf{X}}$ as $\delta$ and the radius of the bond-associated horizon $h_{\mathbf{X}'}$ as $\delta'$, these can be expressed in terms of the mesh spacing $\Delta x$ as $\delta = m \cdot \Delta x$ and $\delta' = m' \cdot \Delta x$, where $m$ and $m'$ are called as spacing factor and bond-associated spacing factor, respectively. When the size of the bond-associated horizon is at least twice as large as the size of material point horizon, that is, $\delta' \geq 2\delta$, the conventional deformation gradient is recovered from Equations (1)–(3).

## 2.2 | Force density state

Given the bond-associated deformation gradient, the bond-associated force density state can be derived from the Fréchet derivative of the bond-associated energy density and by assuming energy equivalency with its continuum counterpart.[6] This results in the same form for the bond-associated force density state as the force density state in the conventional formulation but replacing with bond-associated quantities, which can be written as

$$\underline{\mathbf{T}}_{\xi}[\mathbf{X}, t]\langle\boldsymbol{\xi}\rangle = \nabla W_{\xi}\left(\underline{\mathbf{Y}}\right) = w\langle\boldsymbol{\xi}\rangle \cdot \mathbf{P}_{\xi} \cdot \mathbf{K}_{\xi}^{-1} \cdot \underline{\mathbf{X}}, \tag{4}$$

where $W_{\xi}$ is the bond-associated strain energy density, $\mathbf{P}_{\xi}$ is the bond-associated first Piola–Kirchhoff stress tensor, and $\underline{\mathbf{X}} = \mathbf{X}' - \mathbf{X}$.

The bond-associated strain energy density can be approximated from the strain energy density of a material point using the volume ratio between the subset and the whole material point horizon as

$$W_{\xi}\langle H_{\mathbf{X}} \cap h_{\mathbf{X}'}\rangle = \frac{\int_{H_{\mathbf{X}} \cap h_{\mathbf{X}'}} 1 dV_{\mathbf{X}''}}{\int_{H_{\mathbf{X}}} 1 dV_{\mathbf{X}'}} \cdot W\langle H_{\mathbf{X}}\rangle. \tag{5}$$

As discussed in Section 1, the force density state of a bond should depend on all the bond-associated force density states whose calculation involves the deformation state of the bond. However, a localized force density state that depends only on its own bond-associated force density state is derived in the Form I formulation.[5,6] This has the advantages of simplifying the calculation process while maintaining moderate prediction accuracy. More rationale on this can be found in References 5 and 6. Using the above volume ratio for the strain energy density distribution within a material point horizon, the final force density state of bond in the Form I formulation can be written as

$$\underline{\mathbf{T}}[\mathbf{X}, t]\langle\boldsymbol{\xi}\rangle = \frac{\int_{H_{\mathbf{X}} \cap h_{\mathbf{X}'}} 1 dV_{\mathbf{X}''}}{\int_{H_{\mathbf{X}}} 1 dV_{\mathbf{X}'}} \cdot w\langle\boldsymbol{\xi}\rangle \cdot \mathbf{P}_{\xi} \cdot \mathbf{K}_{\xi}^{-1} \cdot \underline{\mathbf{X}}. \tag{6}$$

As has been demonstrated by different researchers using various numerical examples,[5-12] the bond-associated formulations inherently remove the material instability in the conventional formulation and predicts the results of both static and dynamic deformation problems to certain accuracy by choosing appropriate bond-associated horizon size. However, as was revealed from detailed studies by the authors,[5,6,12] the Form I formulation has some issues with 1D problems and multi-dimensional problems when the bond-associated horizon size is close to the size of material point horizon. This motivates the authors to develop the Form II formulation, in which the force density state of a bond depends on all the bond-associated force density states whose calculation involves the deformation state of the bond. The details of this Form II formulation is presented in the following section.

# 3 | FORM II BOND-ASSOCIATED CORRESPONDENCE FORMULATION

Let's start with the strain energy density increment for a material point in the conventional correspondence formulation.[1] In general, the increment of strain energy density for a material point is a function of the changes of deformation states of all bonds in the horizon of the material point, which is written as

$$\Delta W\left(\underline{\mathbf{Y}}\right) = \int_{H_{\mathbf{X}}} \underline{\mathbf{T}}\left(\underline{\mathbf{Y}}\right) \cdot \boldsymbol{\Delta}\underline{\mathbf{Y}} dV_{\mathbf{X}'}. \tag{7}$$

Similarly, the increment of bond-associated strain energy density for a subset of the material point horizon can be expressed as

$$\Delta W_{\xi}\left(\underline{\mathbf{Y}}'\right)=\int_{H_{\mathbf{X}}\cap h_{\mathbf{X}'}}\underline{\mathbf{T}}_{\xi}\left(\underline{\mathbf{Y}}'\right)\cdot\boldsymbol{\Delta}\underline{\mathbf{Y}}'dV_{\mathbf{X}''}. \tag{8}$$

Therefore, the increment of strain energy density for a material point in the bond-associated formulation can be calculated as the weighted average of all the bond-associated strain energy density increments of all the subsets at the material point, which can be written as

$$\Delta W\left(\underline{\mathbf{Y}}\right)=\sum_{n=1}^{N_H}w'\langle H_{\mathbf{X}}\cap h_{\mathbf{X}'_n}\rangle\cdot\Delta W_{\xi_n}\left(\underline{\mathbf{Y}}'\right), \tag{9}$$

where $N_H$ is the number of material points within a material point horizon, $w'\langle H_{\mathbf{X}}\cap h_{\mathbf{X}'_n}\rangle$ is the weight associated with each bond-associated subset, and $W_{\xi n}$ is the bond-associated strain energy density for the bond-associated subset $H_{\mathbf{X}}\cap h_{\mathbf{X}'_n}$. The subscript $n$ indicates the $n$th material point in the material point horizon.

One possible form of the weight function $w'$ is given in terms of the volume ratio of the bond-associated subset to the sum of all subsets of a material point horizon, which is written as

$$w'\langle H_{\mathbf{X}}\cap h_{\mathbf{X}'_n}\rangle=\frac{\int_{H_{\mathbf{X}}\cap h_{\mathbf{X}'_n}}1dV_{\mathbf{X}''}}{\sum_{m=1}^{N_H}\left(\int_{H_{\mathbf{X}}\cap h_{\mathbf{X}'_m}}1dV_{\mathbf{X}''}\right)}. \tag{10}$$

Based on Equations (7)–(9), the following relationship between all the force density states within a material point horizon and all the bond-associated force density states within the same material point horizon can be established as,

$$\int_{H_{\mathbf{X}}}\underline{\mathbf{T}}\left(\underline{\mathbf{Y}}\right)\cdot\boldsymbol{\Delta}\underline{\mathbf{Y}}dV_{\mathbf{X}'}=\sum_{n=1}^{N_H}\left(w'\langle H_{\mathbf{X}}\cap h_{\mathbf{X}'_n}\rangle\cdot\int_{H_{\mathbf{X}}\cap h_{\mathbf{X}'_n}}\underline{\mathbf{T}}_{\xi}\left(\underline{\mathbf{Y}}'\right)\cdot\boldsymbol{\Delta}\underline{\mathbf{Y}}'dV_{\mathbf{X}''}\right). \tag{11}$$

For the right-hand side of Equation (11), it can be recast by collecting all the terms corresponding to the same deformation state as the left-hand side as

$$\begin{aligned}
&\sum_{n=1}^{N_H}w'\langle H_{\mathbf{X}}\cap h_{\mathbf{X}'_n}\rangle\cdot\int_{H_{\mathbf{X}}\cap h_{\mathbf{X}'_n}}\underline{\mathbf{T}}_{\xi}\left(\underline{\mathbf{Y}}'\right)\cdot\boldsymbol{\Delta}\underline{\mathbf{Y}}'dV_{\mathbf{X}''}\\
&=\sum_{n=1}^{N_H}\left(w'\langle H_{\mathbf{X}}\cap h_{\mathbf{X}'_n}\rangle\cdot\sum_{m=1}^{N_h}\underline{\mathbf{T}}_{\xi_m}\left(\underline{\mathbf{Y}}'\right)\cdot\boldsymbol{\Delta}\underline{\mathbf{Y}}'_m\cdot\Delta V_{\mathbf{X}''_m}\right)\\
&=\sum_{n=1}^{N_H}\left(\sum_{m=1}^{N_b}w'\langle H_{\mathbf{X}}\cap h_{\mathbf{X}'_m}\rangle\cdot\underline{\mathbf{T}}_{\xi_m}\left(\underline{\mathbf{Y}}'\right)\right)\cdot\boldsymbol{\Delta}\underline{\mathbf{Y}}_n\cdot\Delta V_{\mathbf{X}'_n}\\
&=\int_{H_{\mathbf{X}}}\left(\sum_{m=1}^{N_b}w'\langle H_{\mathbf{X}}\cap h_{\mathbf{X}'_m}\rangle\cdot\underline{\mathbf{T}}_{\xi_m}\left(\underline{\mathbf{Y}}'\right)\right)\cdot\boldsymbol{\Delta}\underline{\mathbf{Y}}\cdot dV_{\mathbf{X}'},
\end{aligned} \tag{12}$$

where $N_h$ is the number of material points in the subset of material point $\mathbf{X}'_n$ and $N_b$ is the number of material points whose subset includes the material point $\mathbf{X}'_n$. In general, $N_h\neq N_b$, and any relationship between $N_h$ and $N_b$ does not affect the results of Equation (12). For the case of uniform bond-associated horizon size, $N_h=N_b$, since a material point is in the bond-associated subsets of all material points that fall in its own bond-associated subset. It should also be noted that the bond-associated force density states in the last equation of (12) are formulated based on different bond-associated subsets that include the material point $\mathbf{X}'$ of $\boldsymbol{\Delta}\underline{\mathbf{Y}}$, which makes it impossible to express the force density state in the proposed Form II formulation in the form of integral but as finite summation of all the bond-associated force density states.

Therefore, the following relationship is obtained after replacing the right-hand side of Equation (11) with Equation (12),

$$\underline{\mathbf{T}}\left[\mathbf{X},t\right]\langle\boldsymbol{\xi}\rangle=\sum_{n=1}^{N_b}w'\langle H_{\mathbf{X}}\cap h_{\mathbf{X}'_n}\rangle\cdot\underline{\mathbf{T}}_{\boldsymbol{\xi}_n}\left[\mathbf{X},t\right]\langle\boldsymbol{\xi}\rangle, \tag{13}$$

where $\underline{\mathbf{T}}_{\boldsymbol{\xi}_n}\left[\mathbf{X},t\right]\langle\boldsymbol{\xi}\rangle$ indicates the bond-associated force density state of bond $\boldsymbol{\xi}$ calculated based on the bond-associated subset of the $m$th material point within the bond-associated subset of material point $\mathbf{X}'$ of $\boldsymbol{\xi}$. An illustration of the summation of all the bond-associated force density states of a bond whose force density state is sought is shown in Figure 2. For bond $\boldsymbol{\xi}$, since material point $\mathbf{X}'$ belongs to all the bond-associated horizons of material points who are also within the bond-associated horizon of $\mathbf{X}'$, its force density state has contribution from all the bond-associated force density states of bond $\boldsymbol{\xi}$ calculated based on those bond-associated subsets $H_{\mathbf{X}}\cap h_{\mathbf{X}'_1}$, $H_{\mathbf{X}}\cap h_{\mathbf{X}'_2}$, $H_{\mathbf{X}}\cap h_{\mathbf{X}'_3}$. It should be noted that the bond-associated force density state calculated based on the bond-associated horizon of material point $\mathbf{X}'$ will also contribute to the force density state of bond $\boldsymbol{\xi}$.

Finally, the force density state of a bond $\boldsymbol{\xi}$ in the Form II formulation has the following explicit expression,

$$\underline{\mathbf{T}}\left[\mathbf{X},t\right]\langle\boldsymbol{\xi}\rangle=\sum_{n=1}^{N_b}w'\langle H_{\mathbf{X}}\cap h_{\mathbf{X}'_n}\rangle\cdot w\langle\boldsymbol{\xi}\rangle\cdot\mathbf{P}_{\boldsymbol{\xi}_n}\cdot\mathbf{K}_{\boldsymbol{\xi}_n}^{-1}\cdot\underline{\mathbf{X}}, \tag{14}$$

where $\mathbf{P}_{\boldsymbol{\xi}_n}$ and $\mathbf{K}_{\boldsymbol{\xi}_n}^{-1}$ are respectively the bond-associated first Piola–Kirchhoff stress and the shape tensor in the reference configuration for the bond-associated subset $H_{\mathbf{X}}\cap h_{\mathbf{X}'_n}$ that includes the material point $\mathbf{X}'$ of bond $\boldsymbol{\xi}$.

Comparing the two force density states from Form I and Form II formulations, two observations can be made: First, while the Form I force density state depends on only the bond-associated force density state supported by the subset of the bond, the Form II force density state has contributions from all the bond-associated force density states whose formulation involves the material point of the bond. Second, both Form I and Form II bond-associated formulations recover the conventional formulation when the size of the bond-associated horizon is at least twice as large as the size of the material point horizon. Detailed comparison regarding numerical performance of these two formulations will be carried out in the numerical study section.

The bond-associated formulations share the same equations of motion as the general non-ordinary state-based peridynamics models, which can be written as

$$\rho\left(\mathbf{X}\right)\ddot{\mathbf{u}}\left(\mathbf{X},t\right)=\int_{H_{\mathbf{X}}}\underline{\mathbf{T}}\left[\mathbf{X},t\right]\langle\boldsymbol{\xi}\rangle-\underline{\mathbf{T}}\left[\mathbf{X}',t\right]\langle-\boldsymbol{\xi}\rangle dV_{\mathbf{X}'}+\mathbf{b}\left(\mathbf{X},t\right), \tag{15}$$

where $\rho$ is the mass density, $\mathbf{u}$ is the displacement vector, $\underline{\mathbf{T}}\left[\mathbf{X},t\right]\langle\boldsymbol{\xi}\rangle$ is the force density state that material point $\mathbf{X}'$ exerts on material point $\mathbf{X}$, and $\underline{\mathbf{T}}\left[\mathbf{X}',t\right]\langle-\boldsymbol{\xi}\rangle$ is the force density state that material point $\mathbf{X}$ exerts on material point $\mathbf{X}'$, and $\mathbf{b}$ is the general external force density vector.

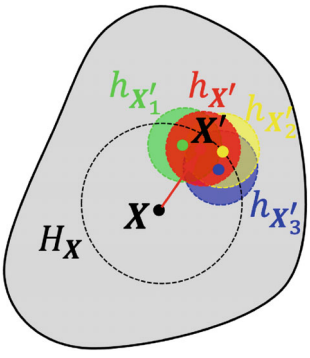


**FIGURE 2** A typical configuration for the calculation of force density state of bond $\boldsymbol{\xi}$ based on all the bond-associated horizons that contain the material point $\mathbf{X}'$.

As has been shown by Silling et al.,[1] the balance of linear momentum is satisfied irrespective to the explicit form of the force density state $\underline{\mathbf{T}}$ as long as the equations of motion are in the form of Equation (15). Therefore, the balance of linear momentum is automatically satisfied in the proposed Form II formulation. For completeness, a proof of balance of angular momentum of the proposed Form II formulation is presented in the Appendix.

## 4 | NUMERICAL STUDY

In this section, detailed investigation and comparison between the Form I and the Form II bond-associated formulations are conducted using three types of problems, namely, wave dispersion analysis, static deformation analysis, and wave propagation analysis. By changing the size of bond-associated horizon relative to the size of material point horizon, its effects on model stabilization and prediction accuracy in both formulations are investigated and compared. Analytical solution (for wave dispersion analysis and 1D static deformation) and finite element method predictions using MOOSE framework[15] and LS-DYNA[16] (for 2D static deformation and wave propagation, respectively) are used as reference solutions, which are plotted in the figures as the solid black curves. Unless otherwise noted, the material properties and model parameters presented in Table 1 are used throughout this section. All the numbers used or reported in this section are dimensionless.

### 4.1 | Wave dispersion analysis

Wave modeled by peridynamic models are in general dispersive due to the finite size of a material point and the nonlocal interaction among material points. The study of wave dispersion relations of peridynamic correspondence models provides an alternative means to investigate their instabilities.[12] In general, the existence of zero angular frequency for non-zero wavenumber is an indication of having zero-energy modes that cause the material instability in the model. In this section, we study and compare the wave dispersion relations between the Form I and the Form II bond-associated formulations. As pointed out in a recent study by Chan and Chen,[12] the wave dispersion relations of 3D problems are consistent with that of 2D problems in the Form I formulation. Therefore, the focus of this example is on the wave dispersion relations using 1D and 2D problems.

To obtain the wave dispersion relations in the bond-associated formulations, a plane wave of the form[17-19]

$$u(\mathbf{X}, t) = u_0 e^{i(k\mathbf{n}\cdot\mathbf{X}-\omega t)}, \tag{16}$$

is substituted into Equations (6) (Form I) and (14) (Form II) to obtain an algebraic equation systems, with $k$ being wave number, $\mathbf{n}$ is unit vector in the direction of wave propagation, and $\omega$ is angular frequency. The solution procedure and analytical expression of the angular frequency in terms of the wavenumber for the Form I formulation can be found in Reference 12. The same procedure is applied to obtain the wave dispersion relations in the Form II formulation. In this study, we present the final results of the wave dispersion relations in both formulations without details on the derivation. Interested readers could find many papers on this topic, such as References 12,17-19.

**TABLE 1** Material properties and model parameters used in numerical study.

| | | | |
|---|---|---|---|
| Young's modulus $E$ | $10^6$ | | |
| Poisson's ratio $\nu$ | 0.3 | | |
| Density $\rho$ | 100 | | |
| Mesh spacing $\Delta x$ | 1.0 | | |
| Weight function $w\langle\xi\rangle$ | $\delta/\lvert\xi\rvert$ | | |
| Spacing factor $m$ | 2 | 3 | 4 |
| Spacing factor $m'$ | 2, 3, 4 | 3, 4, 5, 6 | 4, 5, 6, 7, 8 |

For all results presented in this section, the angular frequencies are normalized by the theoretical wave propagation speed, $c = \sqrt{\frac{E}{\rho}}$ for 1D problems and $c = \sqrt{\frac{E(1-\nu)}{\rho(1+\nu)(1-2\nu)}}$ for 2D problems. The wavenumber is normalized by $2\pi/\Delta x$. Due to existence of periodicity, the range of the normalized wavenumber is fixed to be one period $[0, 1]$.

## 1D cases

The results of the wave dispersion relations in the 1D Form I and Form II models are shown in Figure 3. It should be noted that since only the real solutions of the angular frequency provide meaningful insights regarding the stability of the correspondence models, the complex solutions if any are treated as zero in the wave dispersion curves. This can be seen from the plots for the Form I models in Figure 3. Also, the intersections at $k\Delta x/2\pi = 1$ is due to the periodicity of the wave dispersion relations resulted from using regular spatial discretization. The solid black lines indicate analytical solution from linear elasticity.

As can be seen from Figure 3, for Form I formulation, all curves for different combinations of the bond-associated horizon size and the material point horizon size show zero angular frequencies for non-zero wavenumbers, except two cases of $m = 3, m' = 3$ and $m = 4, m' = 4$. This indicates the existence of zero-energy modes in the Form I formulation for these combinations. For Form II formulation, the model stability is significantly improved compared to the Form I formulation. Also, there is no complex solution for any combinations, and the number of the occurrence of zero angular frequency for non-zero wavenumber significantly reduced. Except the conventional

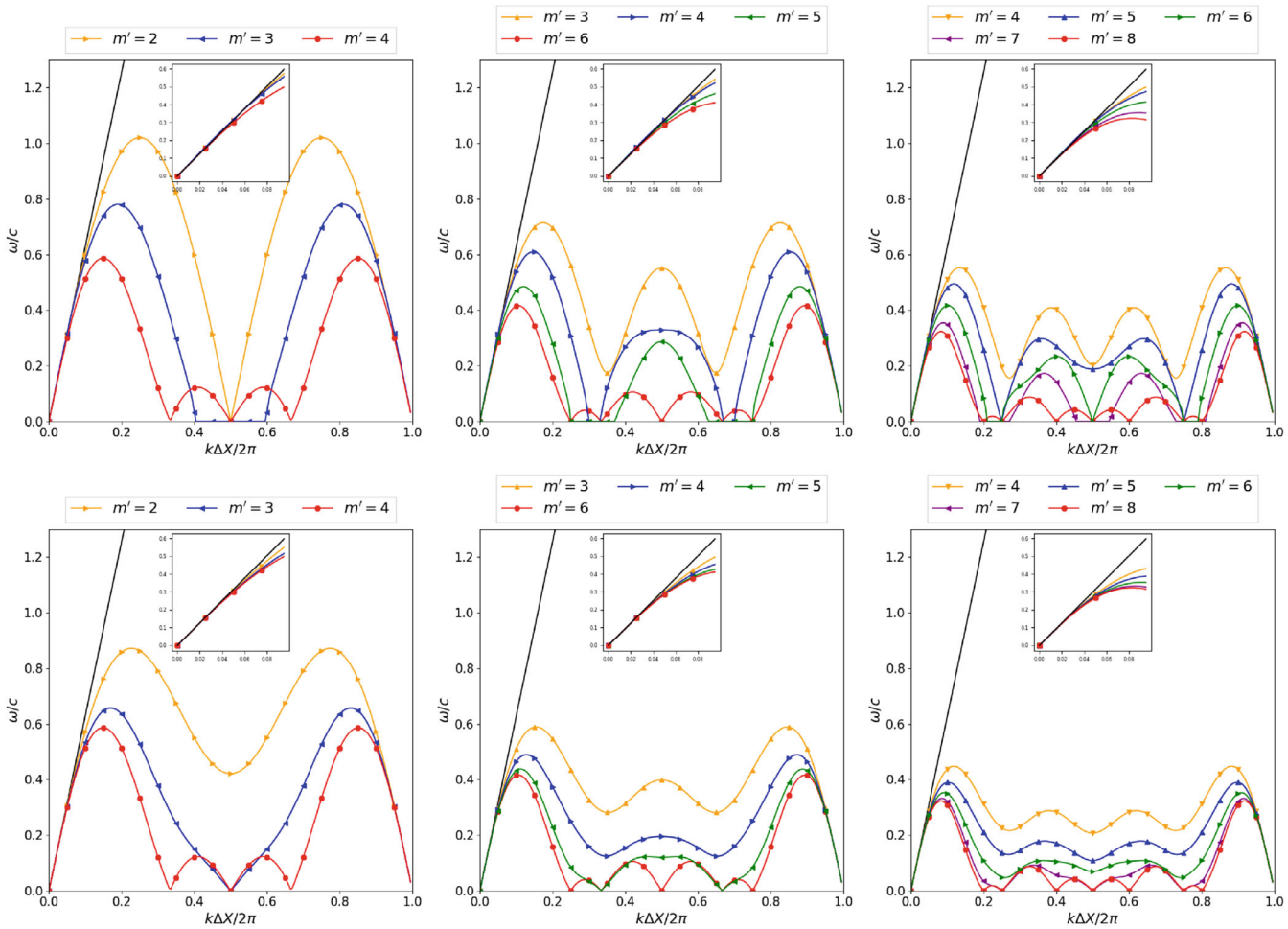


**FIGURE 3** Comparison of 1D wave dispersion relations in bond-associated models for different combinations of horizons (top row: Form I, $m = 2, 3, 4$; bottom row: Form II, $m = 2, 3, 4$).

formulation, zero-energy modes only exist in the Form II formulation for the following combinations: $m = 2, m' = 3$; $m = 3, m' = 5$; and $m = 4, m' = 7$. For both formulation, with the increase of material point horizon, the number of the occurrence of zero angular frequency for non-zero wavenumber increases. Another significant improvement of the Form II formulation over the Form I formulation is the initial slope of the wave dispersion curve. As can be seen from the zoom-in views, the initial slope of some curves are larger than the slope of the theoretical curve. However, all Form II models predict equal or smaller initial slope as that of the theoretical curve.

## 2D cases

For 2D wave dispersion analysis, the incidence angle is set to zero, that is, $\mathbf{n} = [1, 0, 0]$. For this wave propagation direction, there are two roots of the angular frequencies corresponding to the pressure wave and shear wave in the $x$ and $y$ directions, respectively. In this section, only the solution of the pressure wave is studied. Plane stress conditions are assumed. The results for both bond-associated formulations are presented in Figure 4.

As can be seen from Figure 4, material instability is completed removed in the Form II formulation for all the cases studied, while the Form I formulation still suffers from material instability for the case of $m = 2, m' = 3$. This further justifies the findings regarding the material stability of the Form I formulation in the literature, such as References 6 and 5. The issue of the initial slope of the wave dispersion curves of Form I models does not exist for 2D problems.

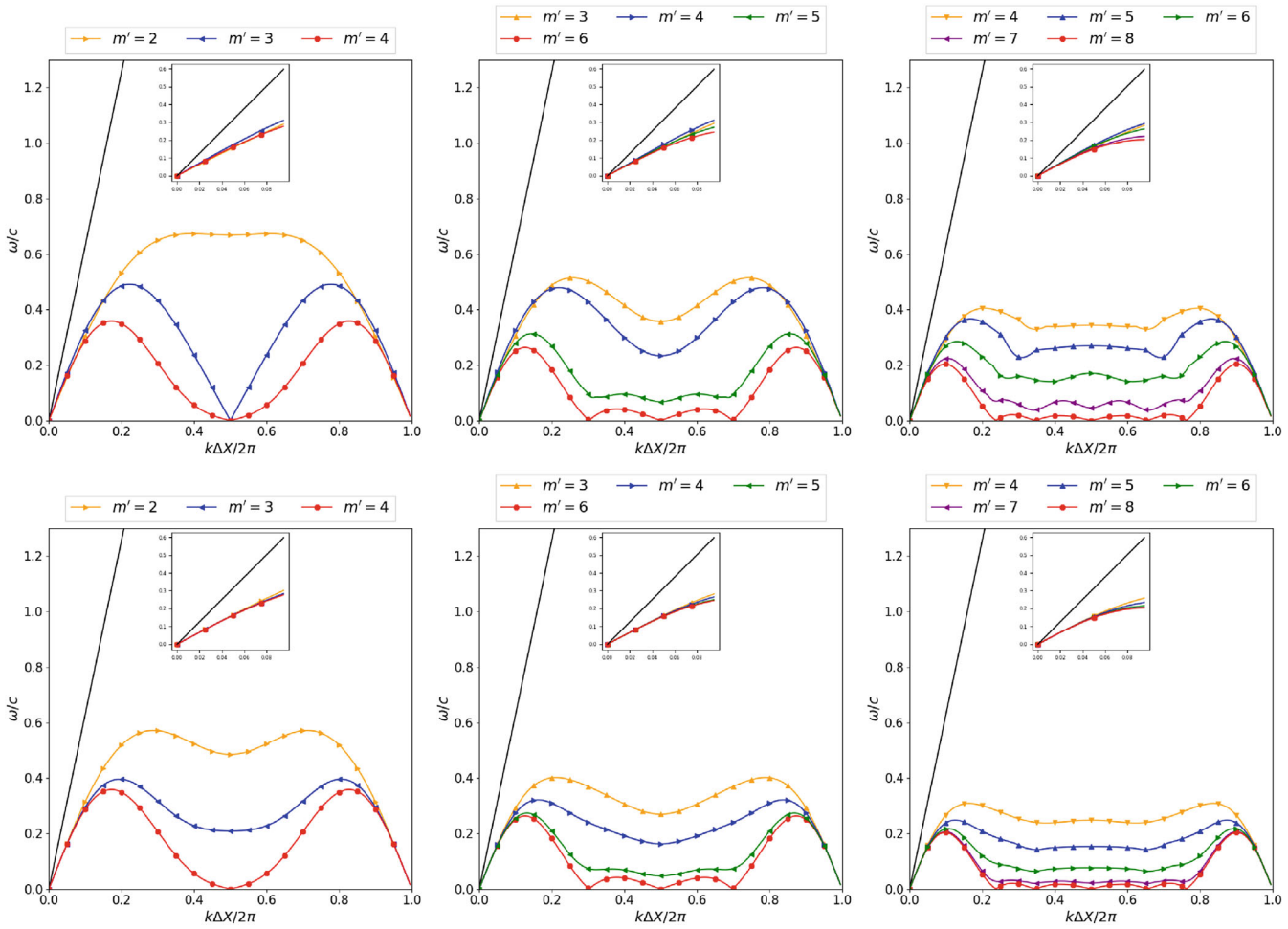


**FIGURE 4** Comparison of 2D wave dispersion relations in bond-associated models for different combinations of horizons (top row: Form I, $m = 2, 3, 4$; bottom row: Form II, $m = 2, 3, 4$).

## 4.2 | Linear elastic deformation analysis

In this example, we investigate and compare the stability and prediction accuracy of the two bond-associated formulations using 1D and 2D static deformation problems. To verify the accuracy of the predictions, the analytical solution (1D) and FEM results (2D) are used as a reference. In addition to detailed comparison with the reference solutions, a global relative error in overall prediction accuracy is also calculated, which is defined as

$$\text{Error} = \frac{\sqrt{\int_\Omega |u_{pd} - u_r|^2 dV}}{\sqrt{\int_\Omega |u_r|^2 dV}}, \tag{17}$$

where $u_{pd}$ is the solution obtained using the two formulations and $u_r$ is the reference solution. The calculated global relative errors for both 1D and 2D problems are tabulated in Table 2, with the errors of the conventional formulation that recovered from bond-associated formulations highlighted. Due to larger oscillation in the displacement fields predicted by the conventional model, these results are not shown in the plots.

### 1D bar

An 1D elastic bar of length $L = 1$ is fixed at one end while the other end is applied with a tensile force of value $2.0 \times 10^4$. The mesh spacing used is $\Delta x = 5.0 \times 10^{-3}$, which results in 200 uniformly spaced material points. The comparison of the displacement field predicted by the two bond-associated formulations are shown in Figure 5. The predicted displacement $u$ and the material point position $x$ are normalized by $\sigma L/E$ and $L$, respectively. For better comparison, the normalized displacement is plotted over the interval of $[0, 1]$.

Based on the results presented in Figure 5, the following observations can be made for 1D static deformation problems. First, as manifested in the form of oscillatory displacement fields, material instability still exists in both bond-associated formulations for certain combinations of the horizon sizes. For the Form I model, these combinations are: $m = 2$, $m' = 2, 3$; $m = 3, m' = 4, 5$; and $m = 4, m' = 5, 6, 7$. For the Form II model, the unstable cases are: $m = 2, m' = 3$; $m = 3, m' = 5$; and $m = 4, m' = 7$. This is consistent with the findings from the wave dispersion analysis. Second, in terms of the slope of the curves, the Form I formulation predicts smaller slope than that of the analytical solution, while the Form II formulation predicts the same slope as that of the analytical solution. This indicates the force density state in

**TABLE 2** Global error for the 1D and 2D static deformation examples

| | | 1D | | 2D | |
|---|---|---|---|---|---|
| $m$ | $m'$ | I | II | I | II |
| 2 | 2 | 0.0380 | 0.0012 | 0.1092 | 0.0055 |
| | 3 | 0.1088 | 0.2057 | 0.2589 | 0.0050 |
| | 4 | 23.4712 | 23.4712 | 0.0283 | 0.0283 |
| 3 | 3 | 0.0505 | 0.0088 | 0.0167 | 0.0046 |
| | 4 | 0.0848 | 0.0143 | 0.1314 | 0.0073 |
| | 5 | 4.1794 | 0.4564 | 0.0647 | 0.0198 |
| | 6 | 16.6490 | 16.6490 | 1.4258 | 1.4258 |
| 4 | 4 | 0.0533 | 0.0210 | 0.0091 | 0.0114 |
| | 5 | 0.0857 | 0.0249 | 0.1276 | 0.0150 |
| | 6 | 0.1153 | 0.0448 | 0.1117 | 0.0220 |
| | 7 | 0.4089 | 0.7748 | 0.0292 | 0.0707 |
| | 8 | 174.1590 | 174.1590 | 1.9212 | 1.9212 |

*Note*: These combinations indicate the results are for the conventional model that recovered from Form I and Form II models, and also show the significant improvement of both Form I and Form II model over the conventional model (in shaded part).

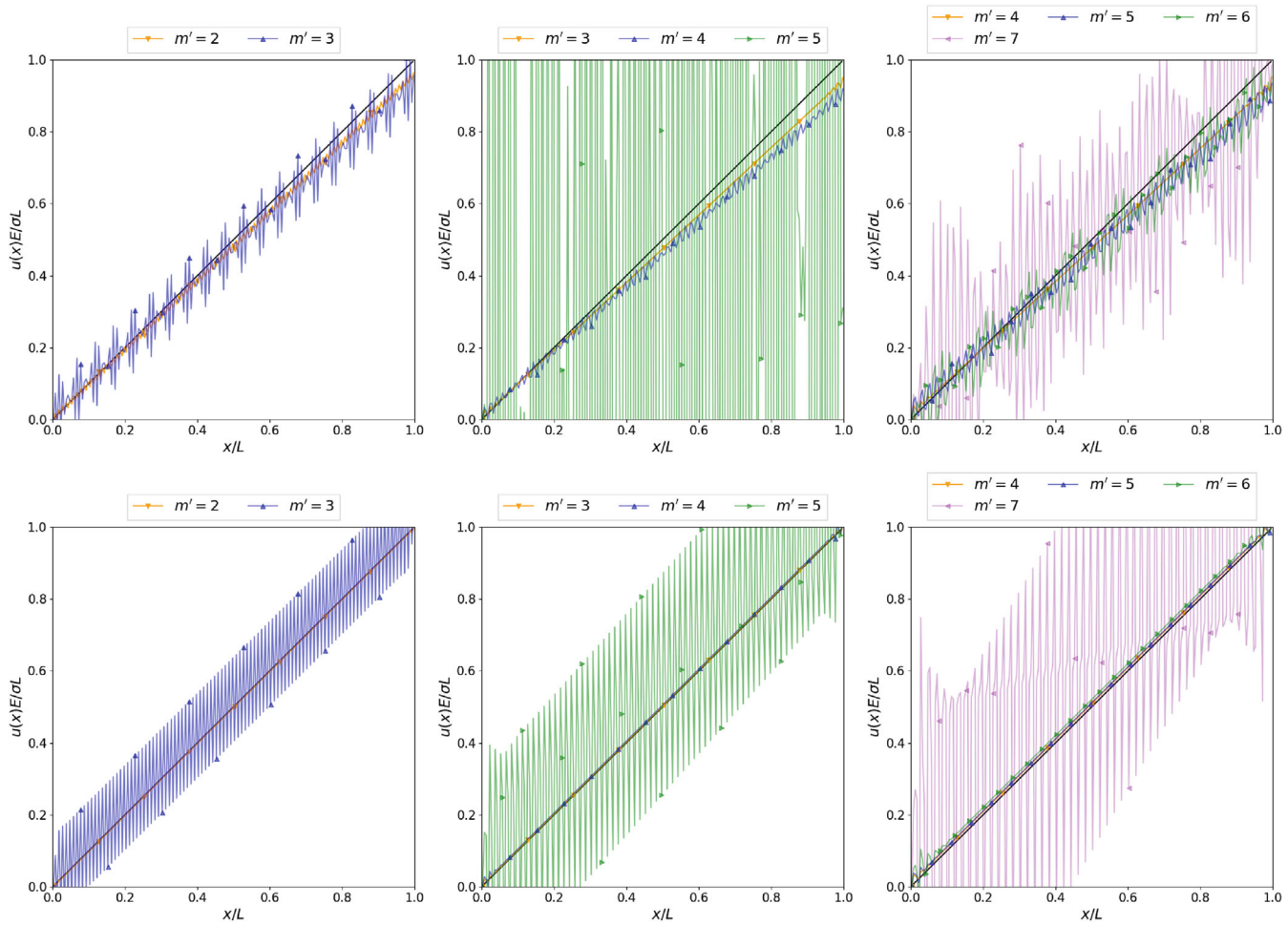


**FIGURE 5** Comparison of displacement $u_x$ of 1D linear elastic bar predicted by the bond-associated models for different combinations of horizons (top row: Form I, $m = 2, 3, 4$; bottom row: Form II, $m = 2, 3, 4$).

the Form I formulation yields larger material stiffness while the force density state in the Form II formulation predicts the correct material stiffness. Third, the oscillations at the beginning and the ending portions of some curves for both bond-associated formulations are due to the well-known *skin effect* when the displacement boundary condition is applied to a single layer of material points. This *skin effect* intensifies with the increase of the material point horizon size. Nonetheless, compared to the Form I formulation, the Form II formulation significantly improves the material instability for 1D problems. For larger bond-associated horizon size, for example, $m' = 2m - 1$, the Form II formulation still has material instability. Although not shown in the plots, the conventional formulation (when $m' = 2m$) has the most significant material instability, which can be seen from the global relative errors presented in Table 2.

The global relative errors shown in Table 2 further support the above observations. For both formulations, the combination of $m = m'$ has the smallest global relative error for a fixed $m$. For each combination, the Form II formulation generally predicts more accuracy result than the Form I formulation.

## 2D rectangular plate with center notch

In this example, a thin rectangular elastic plate with a center notch under plane stress conditions is considered. This example aims to investigate the bond-associated formulations for multi-dimensional problems. The dimensions and boundary conditions of the plate are shown in Figure 6. With regard to spatial discretization, 200 material points along the $x$-direction and 80 material points along the $y$-direction are used, which results in a mesh spacing of $\Delta x = 0.5$. A detailed comparison of displacement $u_x$ along the center line (see dashed line in Figure 6) is made among the two bond-associated formulations and the FEM. To generate the FEM results, 16,000 ($200 \times 80$) 4-node quadrilateral elements with edge length

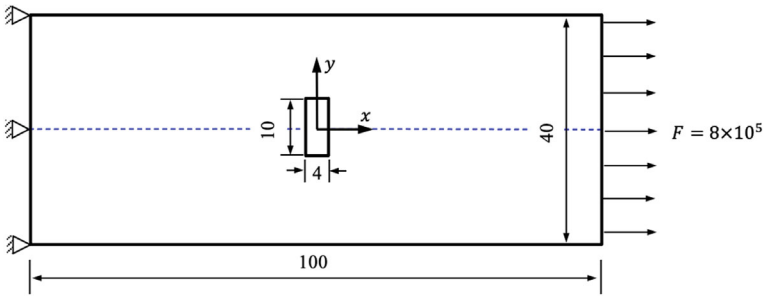


**FIGURE 6** Schematic showing geometry and boundary conditions of a thin rectangular plate with a center notch

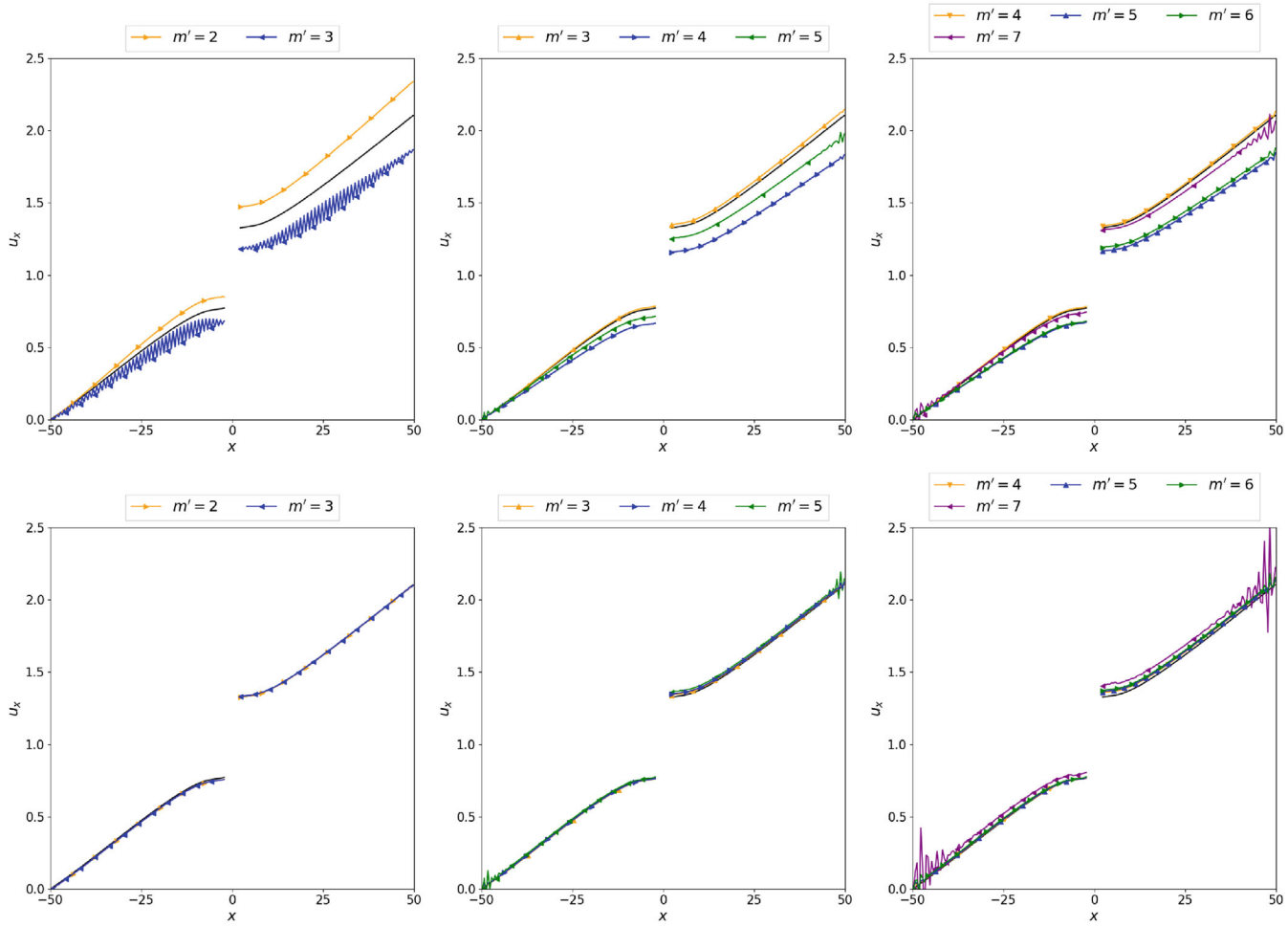


**FIGURE 7** Comparison of displacement $u_x$ along center line predicted by the bond-associated models for different combinations of horizons (top row: Form I, $m = 2, 3, 4$; bottom row: Form II, $m = 2, 3, 4$).

$L_e = 0.5$ were used. The FEM results are shown as solid black curves. The results for the bond-associated models are taken as the average of the solutions at the top and bottom rows of material points closest to the center line. These results are shown in Figure 7. The global relative errors are presented in Table 2. A comparison of the predicted displacement fields of the whole plate using FEM, conventional formulation ($m = 3$), and bond-associated formulations ($m = 3, m' = 3$) are shown in Figure 8.

Based on the results presented in Figure 7, the following observations can be made for 2D static deformation problems. First, the static deformation results are consistent with the wave dispersion analysis results in terms of model instability. For 2D problems, there is only one case, that is, $m = 2, m' = 2$, among all the combinations studied in this work that has

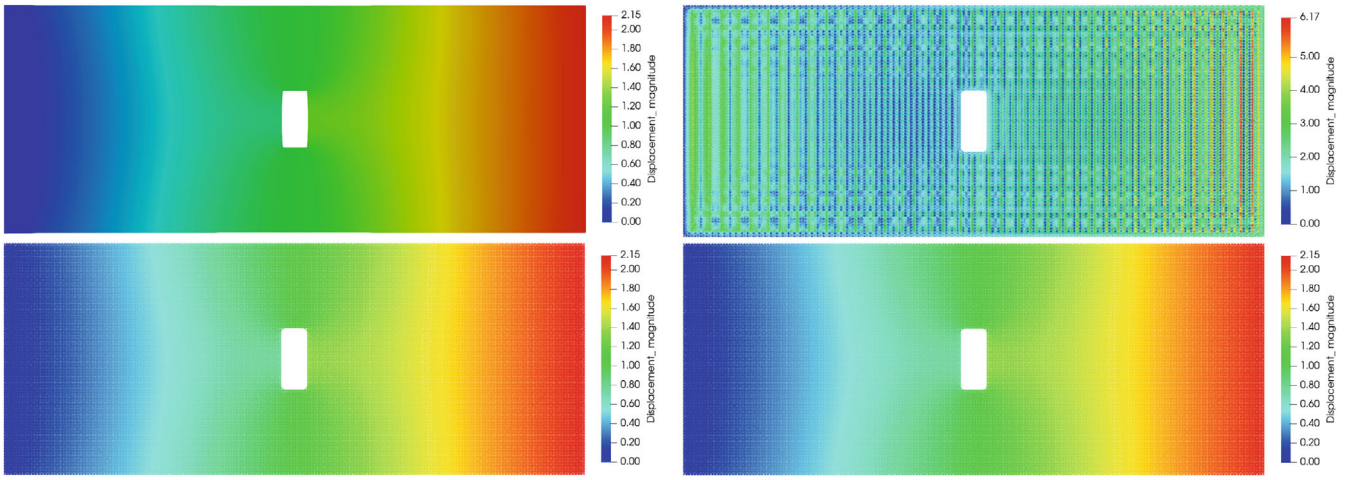


**FIGURE 8** Comparison of the predicted displacement fields of the whole plate (top row: FEM, Conventional $m = 3$; bottom row: Form I, Form II, $m = 3, m' = 3$).

the issue of material instability. Second, compared to the Form I formulation, the Form II formulation is less sensitive to the size of the bond-associated horizon for a fixed material point horizon. This can be seen from the results as all the curves for the Form II models are very close to the FEM curves while the curves for the Form I models are quite scattered away from each other. Third, regarding the *skin effect*, it is more critical in the Form II formulation than in the Form I formulation as both the material point horizon size and the bond-associated horizon size increase. This can be seen for the case of $m = 4, m' = 7$ in Figure 7. The global relative errors presented in Table 2 further confirms that the Form II models perform better than the Form I models, as the errors of the Form II models are significantly smaller than those of the Form I models. The oscillation in the displacement field due to material instability in the conventional model can be seen from Figure 8 for the case of $m = 3$. Compared to the FEM result, both bond-associated formulations predict very accurate displacement field for the case of $m = 3, m' = 3$.

## 4.3 | Wave propagation analysis

The last example investigates and compares the performance of both bond-associated formulations for 3D elastic wave propagation problems. An elastic bar with dimensions of $1.0 \times 1.0 \times 15.0$ is considered. The mesh spacing used in this example is approximately $\Delta x = 0.04762$, which results in 21, 21, and 315 regular material points along the $x$, $y$, and $z$ directions, respectively. The first layer of material points at one end of the elastic bar in the $z$-direction is fixed, while the other end is applied with a displacement

$$u_z(t) = 0.01 \times \sin(40\pi t), \tag{18}$$

for a period of time $t_{apply} = 0.05$. The total simulation time is $t_{total} = 0.35$, and a time step size of $\Delta t = 10^{-4}$ is used. As for time integration, the Verlet method is used. To minimize the effect of the transverse wave on the longitudinal wave due to Poisson's effect, the material Poisson's ratio used in this example is $\nu = 0.0$. The displacement profile of the center material point with coordinates of $(0.5, 0.5, 7.5)$ is shown in Figure 9. For the generation of FEM results, 120,000 ($20 \times 20 \times 300$) 8-node hexahedral elements with edge length $L_e = 0.05$ were used. The FEM results are shown as solid black curves. The vertical dashdotted line indicates the time when the wave hits the other end of the bar.

Based on the results presented in Figure 9, the following observations can be made for wave propagation in the bond-associated models. First, compared to the conventional formulation, both bond-associated formulations improve the stability of the correspondence model for dynamic problems, especially the Form II formulation. For Form I formulation, it underperforms the conventional formulation when $m = 2$. Second, there exists significant phase difference, both lag and lead, in the Form I results compared to the FEM result. However, the Form II models predict much better results than the Form I models. Except for large bond-associated horizons, that is, for cases of $m = 3, m' = 5$ and $m = 4, m' = 7$,

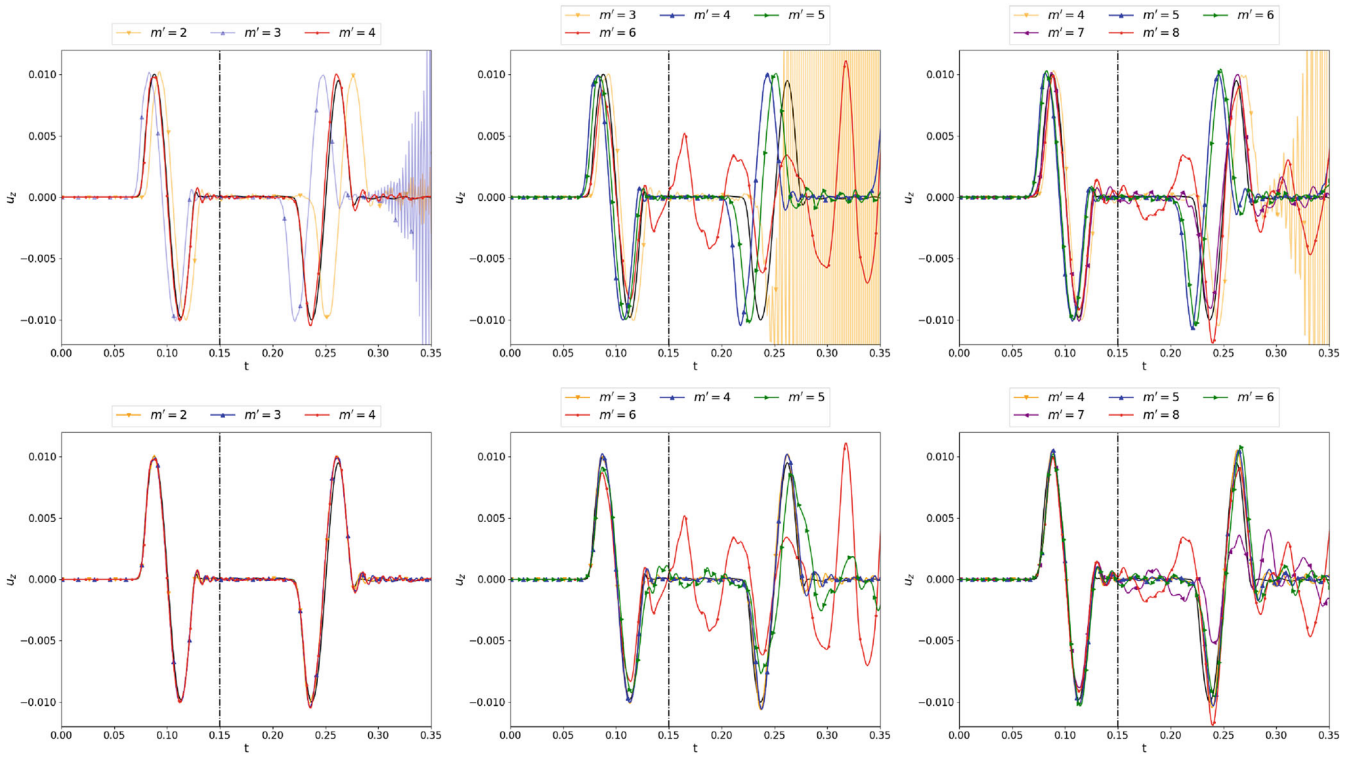


**FIGURE 9** Comparison of displacement profiles at the center material point predicted by bond-associated models for different combinations of horizons (top row: Form I, $m = 2, 3, 4$; bottom row: Form II, $m = 2, 3, 4$).

Form II results correlate to FEM result very well. Third, wave dispersion exists in both bond-associated formulations and it intensifies with the increase of material point horizon size. This applies to all peridynamic models due to the finite size of a material point and the nonlocal interaction among material points. In terms of the displacement profile at the center material point, high-frequency low-magnitude waves are observed after the pass of the main wave, such as at time $t = 0.13$ and $t = 0.28$. The magnitudes of these high-frequency waves increase with the change of material point horizon size from $m = 2$ to $m = 4$. Fourth, there exists dynamic instability in the Form I formulation when the size of the bond-associated horizon is close to the size of the material point horizon, such as $m = 3, m' = 3$. In terms of wave behavior at the center material point, this occurs after the pass of the reflected wave at its location. The interference between the reflected wave and the dispersed wave may be the source of this instability. This dynamic instability is different from the material instability since there is no material instability in the Form I formulation for the cases of $m = 3, m' = 3$ and $m = 4, m' = 4$. Further study is needed to understand this dynamic instability in the Form I formulation. Nonetheless, the Form II formulation does not have such instability and the results of this dynamic example further shows its good performance and high prediction accuracy.

## 5 | DISCUSSION AND CONCLUSION

A reformulation of the peridynamic bond-associated correspondence formulation originally proposed by Chen and Spencer[5,6] was presented and studied in this work. The main difference between the proposed reformulation and the original formulation lies in the calculation of the force density state. In the original formulation, a force density state depends only on the bond-associated force density state of the bond. A volume ratio is used to account for the energy balance between the bond-associated formulation and its continuum counterpart. In the proposed reformulation, a force density state depends on all the bond-associated force density states whose formulation involves the deformation state of the bond. In addition to the material point horizon size, the bond-associated horizon size is also adjustable in the bond-associated formulations. Changing the size of the bond-associated horizon can achieve different degrees of stabilization and results in varying prediction accuracy. Both bond-associated formulations recover the conventional formulation when the bond-associated horizon is at least twice as large as the material horizon.

To investigate and compare the performance of these two bond-associated formulations, three types of problems were studied for different combinations of the size of bond-associated horizon and the size of material point horizon. For wave dispersion analysis, it was found that the reformulation significantly improves the material instability for both 1D and 2D cases. For 1D cases, the initial slope of the wave dispersion curves of the reformulation align well with the theoretical value predicted by linear elasticity, while the original formulation predicts larger initial slope. In addition, the number of occurrence of zero angular frequency for non-zero wavenumber (except those due to periodicity resulted from regular spatial discretization) is greatly reduced. For 2D cases, the material instability for the case of $m = 2, m' = 3$ using the original bond-associated formulation is eliminated in the reformulation. For all other combinations, both bond-associated formulations are free of material instability. The results from static deformation analysis are consistent with the findings from wave dispersion analysis. For 1D cases, the original bond-associated models predict smaller material stiffness than the theoretical value for all combinations. The original bond-associated formulation has material instability for those combinations revealed in the wave dispersion analysis. The reformulation predicts the correct material stiffness and has much smaller global relative errors than the original bond-associated formulation for all combinations without material instability. For 2D cases, both bond-associated formulations predict very good results compared to the FEM solution. The *skin effect* due to missing neighbors for boundary material points becomes more severe in the reformulation than in the original bond-associated formulation with the increase of both material point horizon and the bond-associated horizon. Wave propagation analysis revealed one issue of dynamic instability in the original bond-associated formulation when the size of bond-associated horizon is close to the size of material point horizon. In addition, there is phase difference in the original bond-associated formation depending on the combinations of the size of bond-associated horizon and the size of material point horizon. Wave dispersion in bond-associated formulations is further confirmed in the wave propagation analysis. Based on the numerical investigation and comparison, small bond-associated horizon is recommended for use in the proposed reformulation.

Investigation of the performance of proposed reformulation for fracture problems under various loading conditions is a topic for future work.

## DATA AVAILABILITY STATEMENT

The data that support the findings of this study are available from the corresponding author upon reasonable request.

## ORCID

*WaiLam Chan* https://orcid.org/0000-0003-0616-6231
*Hailong Chen* https://orcid.org/0000-0002-6564-7230

## REFERENCES

1. Silling SA. Peridynamic states and constitutive modeling. *J Elasticity*. 2007;88:42-57. doi:10.1007/s10659-007-9125-1
2. Silling SA. Stability of peridynamic correspondence material models and their particle discretizations. *Comput Methods Appl Mech Eng*. 2017;322:42-57. doi:10.1016/j.cma.2017.03.043
3. Tupek MR, Radovitzky R. An extended constitutive correspondence formulation of peridynamics based on nonlinear bond-strain measures. *J Mech Phys Solids*. 2014;65:82-92. doi:10.1016/j.jmps.2013.12.012
4. Littlewood DJ. Simulation of dynamic fracture using peridynamics, finite element modeling, and contact. Proceedings of the ASME International Mechanical Engineering Congress and Exposition on Mechanics of Solids, Structures and Fluids; Vol. 9; 2010:209-217; ASME.
5. Chen H, Spencer BW. Peridynamic bond-associated correspondence model: stability and convergence properties. *Int J Numer Methods Eng*. 2019;117:713-727. doi:10.1002/nme.5973
6. Chen H. Bond-associated deformation gradients for peridynamic correspondence model. *Mech Res Commun*. 2018;90:34-41. doi:10.1016/j.mechrescom.2018.04.004
7. Gu X, Zhang Q, Madenci E, Xia X. Possible causes of numerical oscillations in non-ordinary state-based peridynamics and a bond-associated higher-order stabilized model. *Comput Methods Appl Mech Eng*. 2019;357:112592. doi:10.1016/j.cma.2019.112592
8. Madenci E, Dorduncu M, Phan N, Gu X. Weak form of bond-associated non-ordinary state-based peridynamics free of zero energy modes with uniform or non-uniform discretization. *Eng Fract Mech*. 2019;218:106613. doi:10.1016/j.engfracmech.2019.106613
9. Behera D, Roy P, Madenci E. Peridynamic correspondence model for finite elastic deformation and rupture in Neo-Hookean materials. *Int J Non-Linear Mech*. 2020;126:103564. doi:10.1016/j.ijnonlinmec.2020.103564
10. Roy P, Behera D, Madenci E. Peridynamic simulation of finite elastic deformation and rupture in polymers. *Eng Fract Mech*. 2020;236:107226. doi:10.1016/j.engfracmech.2020.107226
11. Behera D, Roy P, Madenci E. Peridynamic modeling of bonded-lap joints with viscoelastic adhesives in the presence of finite deformation. *Comput Methods Appl Mech Eng*. 2021;374:113584. doi:10.1016/j.cma.2020.113584

12. Chan WL, Chen H. Peridynamic bond-associated correspondence model: wave dispersion property. *Int J Numer Methods Eng*. 2021;1-16. doi:10.1002/nme.6748
13. Madenci E, Barut A, Futch M. Peridynamic differential operator and its applications. *Comput Methods Appl Mech Eng*. 2016;304:408-451. doi:10.1016/j.cma.2016.02.028
14. Yang S, Gu X, Zhang Q, Xia X. Bond-associated non-ordinary state-based peridynamic model for multiple spalling simulation of concrete. *Acta Mech Sin*. 2021;124. doi:10.1007/s10409-021-01055-5
15. Gaston D, Newman C, Hansen G, Lebrun-Grandié D. MOOSE: a parallel computational framework for coupled systems of nonlinear equations. *Nucl Eng Des*. 2009;239(10):1768-1778. doi:10.1016/j.nucengdes.2009.05.021
16. Reid JD. LS-DYNA examples manual. Livermore Software Technology Corporation; 2001.
17. Butt S, Timothy J, Meschke G. Wave dispersion and propagation in state-based peridynamics. *Comput Mech*. 2017;60:725-738. doi:10.1007/s00466-017-1439-7
18. Nicely C, Tang S, Qian D. Nonlocal matching boundary conditions for non-ordinary peridynamics with correspondence material model. *Comput Methods Appl Mech Eng*. 2018;338:463-490. doi:10.1016/j.cma.2018.04.027
19. Bažant ZP, Luo W, Chau VT, Bessa MA. Wave dispersion and basic concepts of peridynamics compared to classical nonlocal damage models. *J Appl Mech*. 2016;83(11):111004. doi:10.1115/1.4034319


**How to cite this article:** Chan WL, Chen H. Peridynamic bond-associated correspondence model: Reformulation and comparison study. *Int J Numer Methods Eng*. 2022;123(20):4957-4973. doi: 10.1002/nme.7068

## APPENDIX A. BALANCE OF ANGULAR MOMENTUM

In this appendix, we show the balance of angular momentum of the proposed Form II formulation following the original work by Silling et al.[1] on peridynamic correspondence formulation. Following the eq. (42) in Reference 1, the total angular momentum of a peridynamic body can be expressed as

$$\int_{\Omega} \mathbf{y} \times (\rho \ddot{\mathbf{u}} - \mathbf{b})\, dV_{\mathbf{x}} = -\int_{\Omega}\int_{\Omega} \left(\mathbf{y}' - \mathbf{y}\right) \times \underline{\mathbf{T}}\langle \mathbf{X}' - \mathbf{X}\rangle dV_{\mathbf{X}'} dV_{\mathbf{X}}, \tag{A1}$$

where $\mathbf{y}$ and $\mathbf{y}'$ are the positions of material points $\mathbf{X}$ and $\mathbf{X}'$ in the current configuration, respectively. See Figure 1 for reference.

For the proposed Form II bond-associated formulation, the right-hand side of Equation (A1) can be rewritten based on the bond-associated subsets since force density states are defined based on bond-associated subsets only. This is similar to the transformation of the second integration domain of Equation (A1) from $\Omega$ to $H$ in the conventional formulation.

$$\int_{\Omega}\int_{\Omega} \left(\mathbf{y}' - \mathbf{y}\right) \times \underline{\mathbf{T}}\langle \mathbf{X}' - \mathbf{X}\rangle dV_{\mathbf{X}'} dV_{\mathbf{X}} = \int_{\Omega} \sum_{n=1}^{N_{\Omega}} \int_{H_{\mathbf{X}} \cap h_{\mathbf{X}'_n}} \underline{\mathbf{Y}}'_n \times \left( w'\langle H_{\mathbf{X}} \cap h_{\mathbf{X}'_n}\rangle \cdot w\langle \boldsymbol{\xi}'_n\rangle \cdot \mathbf{P}_{\xi_n} \cdot \mathbf{K}_{\xi_n}^{-1} \cdot \underline{\mathbf{X}}'_n \right) dV_{\mathbf{X}''} dV_{\mathbf{X}}, \tag{A2}$$

where $N_{\Omega}$ is the number of material points in the whole peridynamic body. It should be noted that a reverse operation of the one used in deriving Equation (12) has been used to arrive at the right-hand side of (A2), that is, the bond-associated force density states of Equation (13) for all material points are regrouped based on the bond-associated subset that the bond-associated force density states are formulated.

If all terms in the summation of Equation (A2) are zero, then the balance of angular momentum is satisfied. Next, we show that an arbitrary term in the summation of Equation (A2) is zero following the work by Silling et al.[1]

$$\begin{aligned}
&\left( \int_{H_{\mathbf{X}} \cap h_{\mathbf{X}'_n}} \underline{\mathbf{Y}}'_n \times \left( w'\langle H_{\mathbf{X}} \cap h_{\mathbf{X}'_n}\rangle \cdot w\langle \boldsymbol{\xi}'_n\rangle \cdot \mathbf{P}_{\xi_n} \cdot \mathbf{K}_{\xi_n}^{-1} \cdot \underline{\mathbf{X}}'_n \right) dV_{\mathbf{X}''} \right)_i \\
&= \epsilon_{ijk} \int_{H_{\mathbf{X}} \cap h_{\mathbf{X}'_n}} \left(\underline{Y}'_n\right)_j \left( w'\langle H_{\mathbf{X}} \cap h_{\mathbf{X}'_n}\rangle w\langle \boldsymbol{\xi}'_n\rangle \left[P_{\xi_n}\right]_{kp} \left[K_{\xi_n}^{-1}\right]_{pr} \left(\underline{X}'_n\right)_r \right) dV_{\mathbf{X}''} \\
&= \epsilon_{ijk} \int_{H_{\mathbf{X}} \cap h_{\mathbf{X}'_n}} \left(\underline{Y}'_n\right)_j \left( w'\langle H_{\mathbf{X}} \cap h_{\mathbf{X}'_n}\rangle w\langle \boldsymbol{\xi}'_n\rangle \left[\tau_{\xi_n}\right]_{kq} \left[F_{\xi_n}^{-1}\right]_{pq} \left[K_{\xi_n}^{-1}\right]_{pr} \left(\underline{X}'_n\right)_r \right) dV_{\mathbf{X}''}
\end{aligned}$$

$$
\begin{aligned}
&= \epsilon_{ijk}\left[\tau_{\xi_n}\right]_{kq}\left[F_{\xi_n}^{-1}\right]_{pq}\left[K_{\xi_n}^{-1}\right]_{pr} w'\langle H_{\mathbf{X}}\cap h_{\mathbf{X}'_n}\rangle \int_{H_{\mathbf{X}}\cap h_{\mathbf{X}'_n}} w\langle \boldsymbol{\xi}'_n\rangle \left(\underline{Y}'_n\right)_j \left(\underline{X}'_n\right)_r dV_{\mathbf{X}''}\\
&= \epsilon_{ijk}\left[\tau_{\xi_n}\right]_{kq}\left[F_{\xi_n}^{-1}\right]_{pq}\left[K_{\xi_n}^{-1}\right]_{pr} w'\langle H_{\mathbf{X}}\cap h_{\mathbf{X}'_n}\rangle \left[F_{\xi_n}\right]_{js}\left[K_{\xi_n}\right]_{sr}\\
&= \epsilon_{ijk}\left[\tau_{\xi_n}\right]_{kq}\left[F_{\xi_n}^{-1}\right]_{pq}\left[F_{\xi_n}\right]_{js}\left[K_{\xi_n}^{-1}\right]_{pr}\left[K_{\xi_n}\right]_{sr} w'\langle H_{\mathbf{X}}\cap h_{\mathbf{X}'_n}\rangle\\
&= \epsilon_{ijk}\left[\tau_{\xi_n}\right]_{kq}\left[F_{\xi_n}^{-1}\right]_{pq}\left[F_{\xi_n}\right]_{js}\delta_{ps} w'\langle H_{\mathbf{X}}\cap h_{\mathbf{X}'_n}\rangle\\
&= \epsilon_{ijk}\left[\tau_{\xi_n}\right]_{kq}\left[F_{\xi_n}^{-1}\right]_{pq}\left[F_{\xi_n}\right]_{jp} w'\langle H_{\mathbf{X}}\cap h_{\mathbf{X}'_n}\rangle\\
&= \epsilon_{ijk}\left[\tau_{\xi_n}\right]_{kq}\delta_{jq} w'\langle H_{\mathbf{X}}\cap h_{\mathbf{X}'_n}\rangle\\
&= \epsilon_{ijk}\left[\tau_{\xi_n}\right]_{kj} w'\langle H_{\mathbf{X}}\cap h_{\mathbf{X}'_n}\rangle\\
&= 0,
\end{aligned}
\tag{A3}
$$

where $\boldsymbol{\tau}$ is the Cauchy stress tensor. Therefore, the balance of angular momentum holds in the proposed Form II bond-associated formulation.